The mysterious optical afterglow spectrum of GRB 140506A at z = 0.889

Fynbo, J.P.U.; Krühler, T.; Leighly, K.; Ledoux, C.; Vreeswijk, P.M.; Schulze, S.; Noterdaeme, P.; Watson, D.; Wijers, R.A.M.J.; Bolmer, J.; Cano, Z.; Christensen, L.; Covino, S.; D'Elia, V.; Flores, H.; Friis, M.; Goldoni, P.; Greiner, J.; Hammer, F.; Hjorth, J.; Jakobsson, P.; Japelj, J.; Kaper, L.; Klose, S.; Knust, F.; Leloudas, G.; Levan, A.; Malesani, D.; Milvang-Jensen, B.; Møller, P.; Nicuesa Guelbenzu, A.; Oates, S.; Pian, E.; Schady, P.; Sparre, M.; Tagliaferri, G.; Tanvir, N.; Thöne, C.C.; de Ugarte Postigo, A.; Vergani, S.; Wiersema, K.; Xu, D.; Zafar, T.

DOI
10.1051/0004-6361/201424726

Publication date
2014

Document Version
Final published version

Published in
Astronomy & Astrophysics

A&A 572, A12 (2014)
DOI: 10.1051/0004-6361/201424726

Astronomy & Astrophysics

The mysterious optical afterglow spectrum of GRB 140506A at $z = 0.889^{\star,\star\star}$

J. P. U. Fynbo[1], T. Krühler[2], K. Leighly[3], C. Ledoux[2], P. M. Vreeswijk[4], S. Schulze[5,6], P. Noterdaeme[7], D. Watson[1], R. A. M. J. Wijers[8], J. Bolmer[9], Z. Cano[10], L. Christensen[1], S. Covino[11], V. D'Elia[12,13], H. Flores[14], M. Friis[10], P. Goldoni[15], J. Greiner[9], F. Hammer[16], J. Hjorth[1], P. Jakobsson[10], J. Japelj[17], L. Kaper[8], S. Klose[18], F. Knust[9], G. Leloudas[1], A. Levan[19], D. Malesani[1], B. Milvang-Jensen[1], P. Møller[20], A. Nicuesa Guelbenzu[18], S. Oates[21], E. Pian[22], P. Schady[9], M. Sparre[1], G. Tagliaferri[11], N. Tanvir[23], C. C. Thöne[21], A. de Ugarte Postigo[21,1], S. Vergani[16], K. Wiersema[23], D. Xu[1], and T. Zafar[20]

(Affiliations can be found after the references)

Received 1 August 2014 / Accepted 17 September 2014

ABSTRACT

Context. Gamma-ray burst (GRB) afterglows probe sightlines to star-forming regions in distant star-forming galaxies. Here we present a study of the peculiar afterglow spectrum of the $z = 0.889$ *Swift* GRB 140506A.

Aims. Our aim is to understand the origin of the very unusual properties of the absorption along the line of sight.

Methods. We analyse spectroscopic observations obtained with the X-shooter spectrograph mounted on the ESO/VLT at two epochs 8.8 h and 33 h after the burst, and with imaging from the GROND instrument. We also present imaging and spectroscopy of the host galaxy obtained with the *Magellan* telescope.

Results. The underlying afterglow appears to be a typical afterglow of a long-duration GRB. However, the material along the line of sight has imprinted very unusual features on the spectrum. First, there is a very broad and strong flux drop below 8000 Å (~4000 Å in the rest frame), which seems to be variable between the two spectroscopic epochs. We can reproduce the flux-drops both as a giant 2175 Å extinction bump and as an effect of multiple scattering on dust grains in a dense environment. Second, we detect absorption lines from excited H I and He I. We also detect molecular absorption from CH^+.

Conclusions. We interpret the unusual properties of these spectra as reflecting the presence of three distinct regions along the line of sight: the excited He I absorption originates from an H II-region, whereas the Balmer absorption must originate from an associated photodissociation region. The strong metal line and molecular absorption and the dust extinction must originate from a third, cooler region along the line of sight. The presence of at least three separate regions is reflected in the fact that the different absorption components have different velocities relative to the systemic redshift of the host galaxy.

Key words. gamma-ray burst: individual: GRB140506A – ISM: abundances – dust, extinction – ISM: molecules

1. Introduction

Gamma-ray bursts (GRBs) have become a powerful tool with which to probe the interstellar medium (ISM) of star-forming galaxies (e.g. Jakobsson et al. 2004b; Prochaska et al. 2007; Fynbo et al. 2009; Krühler et al. 2013). Optical spectroscopy of the afterglows allows the measurement of a wide range of important properties of galaxies such as chemical abundances (Savaglio 2006; Fynbo et al. 2006; Thöne et al. 2013; Sparre et al. 2014), molecular content (Fynbo et al. 2006; Prochaska et al. 2009; Krühler et al. 2013; D'Elia et al. 2014; Friis et al. 2014), and dust extinction (Watson et al. 2006; Li et al. 2008; Elíasdóttir et al. 2009; Prochaska et al. 2009; Perley et al. 2010; Zafar et al. 2011; Schady et al. 2012; De Cia et al. 2013; Covino et al. 2013).

In this paper we present spectroscopic observations of the unusual afterglow of the $z = 0.889$ GRB 140506A. GRB 140506A was detected by *Swift* on 2014 May 6, 21:07:36 UT (Gompertz et al. 2014). The prompt emission was also detected by the Konus and *Fermi* satellites (Jenke 2014; Golenetskii et al. 2014). The burst was relatively long with a T_{90} duration of 111.1 ± 9.6 s and the temporal profile is characterized by a sharp initial peak with an extended tail (Markwardt et al. 2014). These properties are fully within the range of normal long-duration GRBs, but the GRB optical afterglow has very unusual properties as we will discuss here.

The paper is organized in the following way: in Sect. 2 we present our observations, in Sect. 3 our results and in Sect. 4 and Sect. 5 we offer our discussion of the results and conclusions.

2. Observations

On 2014 May 7, with a mid exposure time of 8.8 h post burst, we acquired a medium-resolution spectrum with the X-shooter spectrograph (Vernet et al. 2011) mounted at the ESO/VLT, covering a range of 300−2300 nm (Fynbo et al. 2014). The spectrum was taken under excellent conditions with a photometric sky and a very good seeing of 0.″54 in the R band. The observation was

⋆ Based on observations carried out under prog. ID 093.A-0069(B) with the X-shooter spectrograph installed at the Cassegrain focus of the Very Large Telescope (VLT), Unit 2 – Kueyen, operated by the European Southern Observatory (ESO) on Cerro Paranal, Chile. Part of the observation were obtained with *Magellan* as part of the programme CN2014A-114.

⋆⋆ The reduced spectrum (FITS files) is only available at the CDS via anonymous ftp to cdsarc.u-strasbg.fr (130.79.128.5) or via http://cdsarc.u-strasbg.fr/viz-bin/qcat?J/A+A/572/A12 carried out in two executions of a 4 × 600 s observing block following an ABBA nodding pattern. The slit was re-aligned with the parallactic angle between the two executions of the observing block. The slit widths were 1″.0, 0″.9, and 0″.9 in the UVB, VIS, and NIR arms, respectively. The airmasses at the start and end of the spectroscopic observation were 1.43 and 1.22. For the given instrument setup, the nominal resolution is 5500, 8800, and 5100 in the UVB, VIS, and NIR. As the seeing was smaller than the slit width, the actual resolution is higher than this. For the VIS, we measure the resolution from the width of telluric absorption lines and find it to be 24 km s^{-1} (FWHM). For the UVB and NIR arms we find ≈40 and 42 km s^{-1}. All wavelengths are in vacuum and are corrected for the heliocentric velocity of 18.9 km s^{-1}.

Because of very unusual features in the spectrum, we decided to observe the afterglow again the following night, 33 h after the burst, executing again two 4 × 600 s observing blocks. The setup was the same as for the first epoch spectrum and again with the slit aligned with the parallactic angle. The observing conditions were again excellent with photometric conditions, a seeing of 0″.59 in the *R*-band, and an airmass ranging from 1.27 to 1.21. The X-shooter spectra were reduced using the official ESO pipeline version 2.2.0 (Goldoni et al. 2006; Modigliani et al. 2010).

The Gamma-Ray burst Optical Near-Infrared Detector (GROND, Greiner et al. 2008) mounted on the MPG 2.2 m telescope on La Silla observed the field of GRB 140506A on 2014-05-09, 2014-05-10, and 2014-05-28. A late-time host galaxy observation was carried out on 2014-07-14. Simultaneous photometry was obtained in seven broad-band filters ($g'r'i'z'$ in the optical and JHK_s in the near-infrared wavelength range) with a total integration time of around 90 min in $g'r'i'z'$ and 75 min in JHK_s on each visit. We reduced and analysed the data using custom-made software largely based on pyraf/IRAF (Tody 1993), closely following the procedure outlined in Krühler et al. (2008). Photometric calibration was performed against field stars from the 2MASS catalogue (Skrutskie et al. 2006) in the NIR. The photometry of the optical bands was tied to observations of an SDSS (Aihara et al. 2011) standard field taken immediately before the GRB field. We also use these calibration data for the X-shooter acquisition camera and the *Magellan*/IMACS observations. Details of our photometry are given in Table 1.

Magellan observations were done in the following way. We first obtained a deep image of the field with the f/4 camera on the Inamori-*Magellan* Areal Camera and Spectrograph (IMACS; Dressler et al. 2011) on the *Magellan/Baade* 6.5-m telescope. The observation started at 03:04 UT on June 26, 2014 (i.e. 51.5 days after the GRB) and comprised of three unfiltered images with an individual exposure time of 300 s.

After the host galaxy was detected in the combined image, we acquired a spectrum starting 03:47 UT, comprising of six exposures with an individual integration time of 1200 s (see Fig. 1). At the redshift of the GRB, the emission lines lie in the red part of the visual spectrum. To disentangle them from the sky emission lines, we chose an intermediate-resolution grating with 600 lines/mm and a blaze angle of 15°.4. For the given configuration, the dispersion is 0.39 Å/px, the resolving power is about 3600 and the spectral range extends from 6600 Å to 9770 Å. We chose a slit width of 1″.2 to match the seeing conditions. The *Magellan* data were reduced and calibrated using standard procedures in IRAF (Tody 1993). The extraction aperture had a width of 10 pixels (2″.2). The spectrum was flux-calibrated with the spectrophotometric standard star Feige 56. The wavelength solution was transformed to vacuum wavelengths.

Table 1. Photometry of the afterglow and host galaxy from May, June and July 2014.

Instrument	Filter	UT Start time	Magnitude[a,b] (mag)
X-shooter	*R*	2014-05-07 05:03	21.40 ± 0.08
X-shooter	*R*	2014-05-07 05:19	21.44 ± 0.11
X-shooter	*R*	2014-05-07 06:00	21.69 ± 0.11
X-shooter	*R*	2014-05-08 06:00	22.39 ± 0.09
GROND	g'	2014-05-09 07:18	23.73 ± 0.05
GROND	r'	2014-05-09 07:18	22.57 ± 0.04
GROND	i'	2014-05-09 07:18	22.11 ± 0.05
GROND	z'	2014-05-09 07:18	21.82 ± 0.06
GROND	J	2014-05-09 07:18	21.09 ± 0.13
GROND	H	2014-05-09 07:18	20.88 ± 0.18
GROND	K_s	2014-05-09 07:18	20.82 ± 0.22
GROND	g'	2014-05-10 09:17	23.86 ± 0.19
GROND	r'	2014-05-10 09:17	22.76 ± 0.11
GROND	i'	2014-05-10 09:17	22.37 ± 0.11
GROND	z'	2014-05-10 09:17	22.16 ± 0.14
GROND	J	2014-05-10 09:17	>20.95
GROND	H	2014-05-10 09:17	>20.45
GROND	K_s	2014-05-10 09:17	>19.48
GROND	g'	2014-05-28 04:59	24.71 ± 0.11
GROND	r'	2014-05-28 04:59	24.24 ± 0.10
GROND	i'	2014-05-28 04:59	23.66 ± 0.17
GROND	z'	2014-05-28 04:59	23.13 ± 0.17
GROND	J	2014-05-28 04:59	>21.98
GROND	H	2014-05-28 04:59	>21.38
GROND	K_s	2014-05-28 04:59	>20.43
IMACS	*white*	2014-06-26 03:04	24.27 ± 0.14
GROND	g'	2014-07-14 03:53	>24.8
GROND	r'	2014-07-14 03:53	24.43 ± 0.21
GROND	i'	2014-07-14 03:53	23.70 ± 0.15
GROND	z'	2014-07-14 03:53	23.71 ± 0.23
GROND	J	2014-07-14 03:53	>22.07
GROND	H	2014-07-14 03:53	>21.45
GROND	K_s	2014-07-14 03:53	>20.53

Notes. [(a)] All photometry is given in the AB system, and is not corrected for Galactic foreground reddening. [(b)] Upper limits at 3σ confidence level.

3. Results

3.1. Absorption and emission lines

Based on absorption lines from Fe II, Mg II, Ca II, He I* and H I* we infer a redshift of 0.889 for the burst (Fig. 2). This is confirmed by the detection of [OII] emission from the underlying host galaxy (Fig. 2, top right panel, and Fig. 3) redshifted by 30 km s^{-1} relative to the Ca II absorption lines. From the strength of the [OII] we infer a star formation rate (SFR) of 1 $M_\odot$ yr^{-1} using the relation between [OII] luminosity and SFR in Kennicutt (1998). An SED analysis of the host galaxy based on the host photometry in Table 1 following the procedure in Krühler et al. (2011) yields that the host appears to be a typical GRB host with a stellar mass of $\sim 10^9$ $M_\odot$, $A_V \sim 1$ and with a dust-corrected SFR of a few solar masses per year. As seen in Fig. 1 the host is also detected in the *Magellan* white light image.

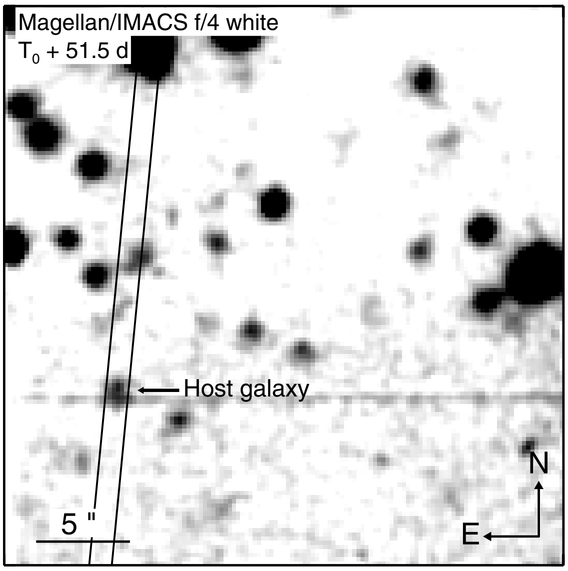

Fig. 1. Field of GRB 140506A (30″ × 30″). The position of the host galaxy is marked. The slit of the late-time spectrum was inclined by −5.°5 east of north. The image has been smoothed with a Gaussian kernel to increase the visibility of the host galaxy.

Table 2. Observer frame equivalent widths for detected lines at both epochs.

Line	EW_1 (Å)	EW_2 (Å)
Fe IIλ2600	2.2 ± 0.9	2.9 ± 1.1
Mg IIλ2796	3.2 ± 0.5	1.9 ± 0.7
Mg IIλ2803	3.7 ± 0.5	2.0 ± 0.7
He I*λ3889	1.13 ± 0.11	1.4 ± 0.3
Ca IIλ3934	2.10 ± 0.11	2.5 ± 0.3
Ca IIλ3969	1.91 ± 0.11	1.6 ± 0.3
Hϵ	0.22 ± 0.05	–
Hδ	0.40 ± 0.05	0.0 ± 0.2
Hγ	0.86 ± 0.05	0.3 ± 0.2
Hβ	0.73 ± 0.05	0.3 ± 0.2
Hα	1.6 ± 0.3	−4.7 ± 1.2
He I*λ10833	5.2 ± 0.5	4.9 ± 1.5
$^{12}CH^+$ λ4233	0.37 ± 0.05	0.38 ± 0.10
[OII]	−1.59 ± 0.13	−3.3 ± 0.3

The *Magellan* spectrum is unfortunately hampered by strong pick-up noise. We detect the [OII] emission line at low signal-to-noise ratio ($\lesssim 3\sigma$), but no other lines are securely detected.

He I* and Balmer line absorption has to our knowledge never been detected before in a GRB optical afterglow spectrum. The measured equivalent widths (EWs) of the main absorption and emission lines are provided in Table 2. The ratio between the EWs of the He I*λ10833 and He I*λ3889 lines is 4.6 ± 0.5. The expected ratio for unsaturated lines from atomic physics is 23.3 indicating significant saturation of at least the He I*λ10833 line. There is evidence for variability of the strength of the Balmer absorption lines. We suspect that this is due to blending with the underlying host emission lines for the following reasons. Firstly, in Table 2 we give the EWs of the [OII] doublet showing that the change in the EWs of emission lines easily are strong enough to cause such an effect. Secondly, the estimated strength of the Balmer emission lines given the SFR would be strong enough. Finally, in the second epoch spectrum there is evidence for Hα emission (see the lower left panel of Fig. 2). Unfortunately Hα is located on a sky line and our

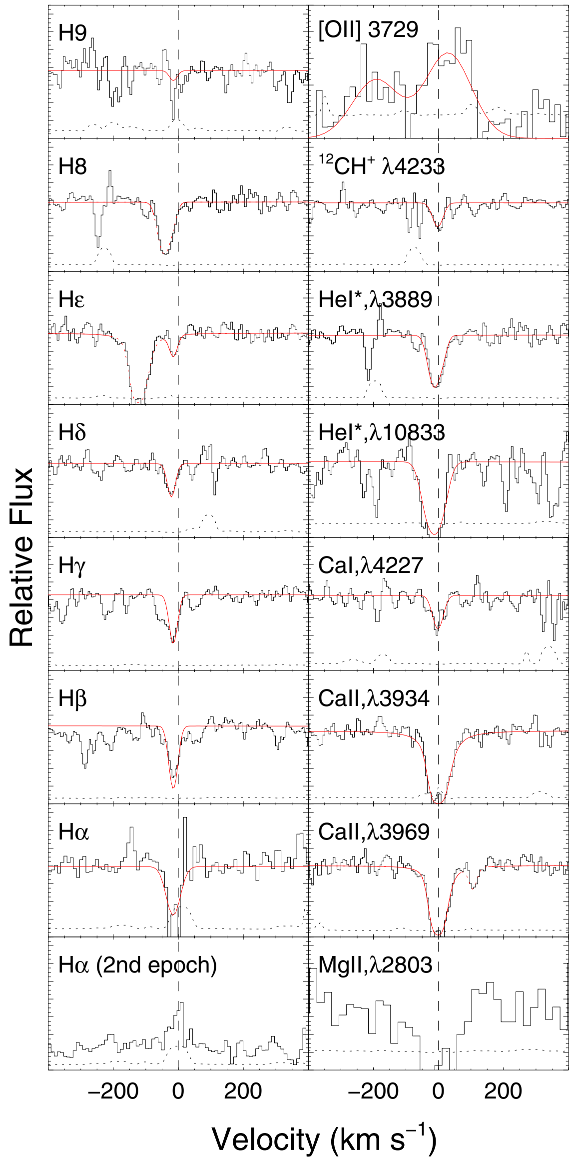

Fig. 2. Main absorption and emission lines in the spectrum. The noise spectra are overplotted with a dotted line and the plot range on the y-axis starts at zero. The scale on the y-axis is arbitrary. The zero point for the velocity scale is set to $z = 0.88911$. In the left column we show the Balmer lines that are centred at -14 km s^{-1} ($z = 0.88902$). For Hα we show the region around the line from both X-shooter spectra. In the right column we show Ca II and Ca I, the He I* lines centred at -11 km s^{-1} ($z = 0.88904$) and the CH^+ line centred at the same velocity as the Ca II lines. We also show the [OII] doublet, which is redshifted by 30 km s^{-1} relative to Ca II and have a velocity width of 150 km s^{-1}. We note that H8 is blended with He I*λ3889. Also overplotted are Voigt profile fits to the absorption lines (except Mg II that is in the UVB part of the spectrum where the signal-to-noise ratio is too low) and a Gaussian fit to the [OII] doublet. For the Ca II lines we only show the Voigt-fits with a single absorption component.

Magellan spectrum is not deep enough so we need a deeper spectrum of the host to be certain about this interpretation of the Balmer line variability.

Finally, we also detect an absorption line consistent with the 4233 Å line from CH^+. There is also a weaker feature consistent with the 3958 Å line. We do not detect absorption from CH. In the MW CH^+ is sometimes stronger than CH (e.g. Smoker et al. 2014) so the detection of CH^+ and nondetection of CH is not unexpected.

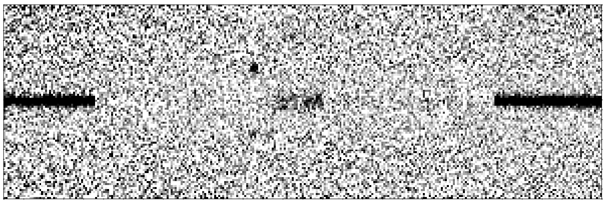

Fig. 3. [O II] emission line doublet from the underlying host galaxy. The afterglow has been subtracted assuming that the afterglow spectrum can be approximated by a linear function across the position of the line (the compact dot above the trace is a cosmic ray hit). Based on the line we infer a star formation rate of 1 $M_{\odot}$ yr^{-1}.

Table 3. Results from Voigt-profile fitting to the lines in the first epoch spectrum.

Element	z	v (km s^{-1})	b (km s^{-1})	log N (log cm^{-2})
H I*	0.88902	−14	8.5 ± 1.5	13.96 ± 0.12
He I*	0.88904	−11	18.5 ± 3.4	13.99 ± 0.12
Ca II	0.88911	0	–	>16.5
Ca I	0.88911	0	16.5 ± 8.0	12.07 ± 0.17
CH$^+$	0.88911	0	16.5 ± 8.0	14.45 ± 0.18

To derive column densities we have carried out Voigt-profile fits of the Balmer, He I*, Ca II, Ca I, and CH$^+$ lines. The results of these fits are provided in Table 3. To obtain acceptable fits we have to adopt different velocity centroids for the calcium and CH$^+$ lines (z = 0.88911), the Balmer lines (z = 0.88902) and the excited helium (z = 0.88904). The uncertainties on the redshifts are 0.00002 so the last two redshifts are marginally consistent. We then tie the Doppler parameters of lines at the same redshifts together and obtain b = 16.5 ± 8.0 km s^{-1} for calcium and CH$^+$, b = 8.5±1.5 km s^{-1} for the Balmer, and b = 18.5±3.4 km s^{-1} for the helium lines respectively. These fits assume a single component per ion/molecule.

For the very strong Ca II($\lambda\lambda$3934, 3969) transitions, in principle, many components with a low column density that are not seen in the weaker lines could contribute to the observed line shape. In an attempt to resolve this ambiguity between total column density and number of components, we fitted the Ca II in such a way that the total number of components was a free parameter in the fit until adding more components did not provide an improvement in the fit statistics. For five unresolved components, for example, the total Ca II column density would be $\log(N/\mathrm{cm}^{-2}) = 16.5 \pm 0.3$. Fits with a fixed number of components (between one and ten) return column densities between $\log(N/\mathrm{cm}^{-2}) \sim 15.8$ and $\log(N/\mathrm{cm}^{-2}) \sim 17.0$. Given the medium resolution of X-shooter and moderate signal-to-noise of our spectra, we cannot make stronger statements on the column density of Ca II.

Voigt profile fits to the second epoch spectrum return within errors consistent results except for the Balmer lines (see also Table 2). Because of the lower signal-to-noise of the second epoch spectrum, however, it does not add substantial extra constraints on the fits. The decreasing equivalent width of the Balmer lines in absorption is likely caused by an increasing contribution of the Balmer lines in emission from the host galaxy.

We have searched for Diffuse Interstellar Bands (e.g. Xiang et al. 2011), but we do not detect any of these above detection limits of $\gtrsim$300 mÅ (3σ).

3.2. The peculiar SED

The spectral energy distribution (SED) is very unusual (Fig. 4): in the NIR and red part of the VIS arm the X-shooter spectrum looks like a typical GRB afterglow, i.e. a power-law spectrum. Then it breaks around 8000 Å (rest frame 4000 Å) and vanishes in the UVB. In Fig. 4 we show the UVB spectrum at λ_{obs} < 4000 Å binned more heavily with red points with error bars. These points indicate a rising trend in the bluest end of the spectra, especially in the second epoch. The flux level in this bluest region of the spectrum is so low (~25 mag on the AB system) that the host galaxy flux is likely to contribute a large fraction of the detected emission. This is clear from Fig. 4 where it can be seen that the flux density of the host galaxy continuum (as traced by the late time GROND photometry shown in orange) is very similar to the flux density in the bluest part of the X-shooter spectra (as shown with red points). However, without more information about the strength of the host emission below 4000 Å it is not possible to judge with certainty whether afterglow emission contributes significantly to the X-shooter spectra below ~4000 Å in the observed frame.

We also reanalysed the imaging data from UVOT. The UVOT photometry shows detections of the afterglow securely in white light and in the U, B and V filters (see also Siegel & Gompertz 2014) during the first few hours after the burst. There is also a tentative detection (2.8σ) in the $UVW1$ band, but only during the first ten minutes after the burst. Overall, the UVOT photometry is consistent with the shape of the SED inferred from the first epoch X-shooter spectrum.

It is important to stress that the X-shooter spectra were taken in excellent conditions so the flux drop in the blue is intrinsic to the event and is not caused by slit-loss. In the following we explore different possible interpretations of this peculiar SED.

3.2.1. A giant 2175-Å extinction bump

The location of the flux-drop is in the rest-frame ultraviolet and it is therefore natural to explore whether this can be an extreme example of the 2175 Å extinction bump known from the Milky Way and also previously seen in GRB afterglow spectra (Ellison et al. 2006; Fynbo et al. 2007; Krühler et al. 2008; Elíasdóttir et al. 2009; Prochaska et al. 2009; Zafar et al. 2011). This feature is ubiquitous in the MW and in M 31. It is also present along sightlines in the LMC and at least one sightline in the SMC (see the extensive discussion of this extinction feature in Elíasdóttir et al. 2009).

The flux drop can be well matched by a Fitzpatrick & Massa (2007) parametrization of the extinction curve except in the bluest region below ~4000 Å. An example is plotted with a solid line in Fig. 4 with these parameters: c_1 = 1.0, c_2 = 0.8, c_3 = 115., c_4 = 0.46, c_5 = 5.9, γ = 2.75, R_V = 3.1, x_c = 4.6, A_V = 0.9. We here assume that the intrinsic spectrum is a power-law $F_\nu \propto \nu^{-\beta}$, with β = 0.75 as derived from the XRT spectrum (β = 0.75 ± 0.07) and with a $\Delta\beta$ = 0.5 break between the X-rays and optical bands. For consistency we have verified that the afterglow lightcurve in the optical and X-ray bands are consistent with a scenario where the cooling break is located between the optical and X-ray bands. The extinction bump is characterized by c_3 and γ. Fitzpatrick & Massa (2007) introduce the bump height $E_{\mathrm{bump}} = c_3/\gamma^2$ and along Milky Way (MW) sightlines E_{bump} and γ are in the range 1–6 and 0.8–1.5, respectively. For GRB 140506A the values are 15 and 2.75, i.e. both are much larger than what is seen along any sightline in the MW.

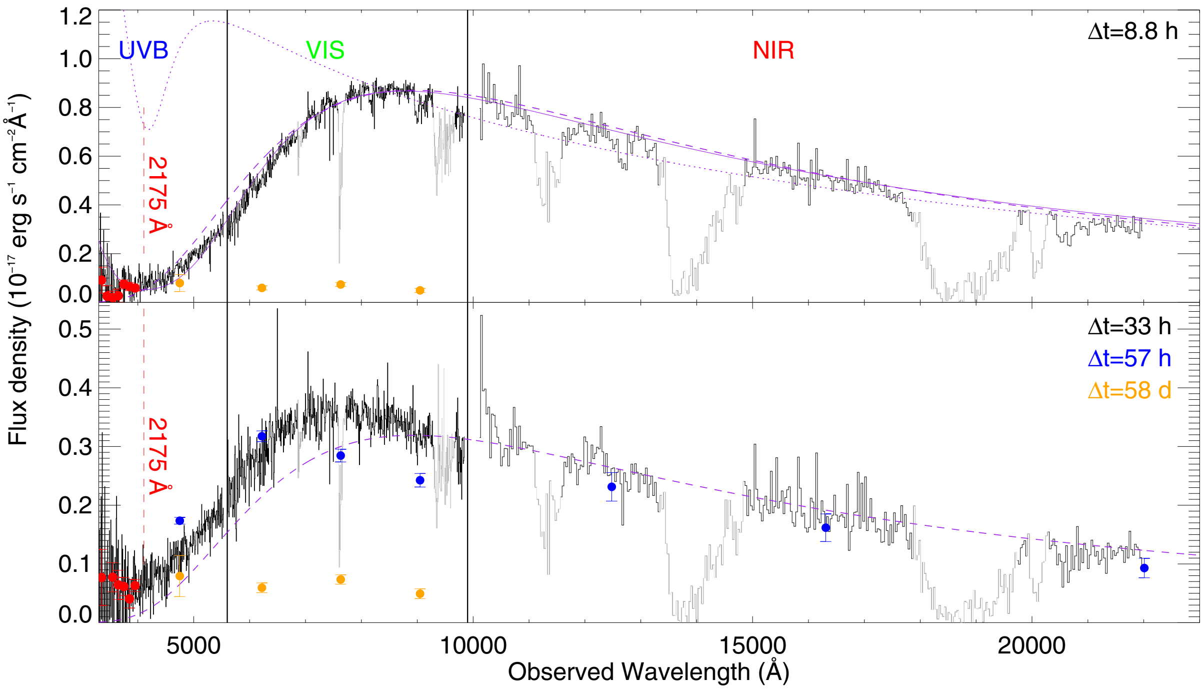

Fig. 4. X-shooter spectra taken 8.8 h (*top*) and 33 h (*bottom*) after the burst. The spectra are binned for better visibility. The red points show the spectrum at $\lambda < 4000$ Å binned in 100 Å bins. Regions affected by telluric absorption are plotted in light grey. Also overplotted on the first epoch spectrum is a power-law (with slope set by a fit to the X-ray afterglow and assuming a $\Delta\beta = 0.5$ cooling break between the X-rays and the optical) reddened by three different prescriptions: MW extinction curve (dotted line), extreme 2175 Å extinction bump (solid line), and extinction with multiple scattering (dashed line). The shape of the second epoch spectrum is generally similar to the spectrum from the first epoch, but the flux drop occurs at slightly bluer wavelengths. To make this clearer we rescale and overplot the modelling of multiple scattering from the first epoch on the spectrum of the second epoch. Furthermore, we show with blue points the GROND photometry from about 57 h after the burst, corrected for host galaxy emission, and with orange points the host photometry from 58 days after the burst.

For comparison we also overplot with a dotted line a Pei (1992) parametrization of the MW extinction curve. Here we have assumed the same underlying power-law spectrum and $A_V = 0.8$. As seen it is here impossible to match the depth and width of the bump. This illustrates well how different the 2175 Å bump has to be from that of the MW.

3.2.2. Extinction with multiple scattering

The extinction feature is also similar to what is seen in rare cases of reddened supernovae and active galactic nuclei (Fynbo et al. 2013; Leighly et al. 2014; Amanullah et al. 2014). These systems have been successfully modelled with the prescription for multiple scattering of light discussed in Wang (2005) and Goobar (2008). The point is here that if the mean free path for dust scattering is smaller than the spatial extent of the dust cloud, the photon propagation is diffusive and the normal single scattering approximation is invalid. The dashed line in Fig. 4 shows a simple model based on this diffusive photon propagation described by the parameters $_V = 0.65$, $p = -2.5$ and $a = 0.8$, which are the relevant parameters for multiple scattering in the case of an underlying LMC-like extinction curve (Goobar 2008). It is not possible to get a good fit with the parameters relevant for an SMC-like extinction curve ($a = 1.0$, $p = -1.07$; Goobar, priv. comm.).

Strictly, the approximation described in Goobar (2008) assumes an isotropically emitting source. As the emission from the GRB afterglow is jetted the details of the effect most likely will be different. It is beyond the scope of the present work to develop a more detailed model of the effective extinction curve in the case of multiple scattering for a jetted source.

3.2.3. SED variation

The shape of the flux drop in the blue end of the spectrum changes between the two epochs. In the lower panel of Fig. 4 we overplot the modelling of multiple scattering from the first epoch on the spectrum of the second epoch which clear shows the change. The shape of the second epoch spectrum is generally similar to the spectrum from the first epoch, but the flux drop occurs at slightly bluer wavelengths. We also overplot on the second epoch spectrum the GROND photometry from about 57 h after the burst indicating an even weaker flux drop at this time.

A contributing cause to this is SED variation could be a changing relative contribution from the underlying host galaxy, but as the host galaxy only contributes 5 and 16% of the total light in the r-band (see Table 1) the host galaxy emission is insufficient to explain the full variation. We return to this point below.

4. Discussion

4.1. Origin and variability of the flux drop

The most remarkable property of the afterglow spectrum is the strong, apparently variable flux drop bluewards of about 8000 Å in the observer frame. Whereas some of the variation of the shape of the flux drop may be explained by an increasing host contribution, in particular from the second epoch spectrum to the GROND photometry the following night, the host is too faint at 24.4 mag in the r band to explain the variation between our two spectroscopic epochs (see afterglow magnitudes in Table 1). More specifically, we concluded this by establishing that the second epoch spectrum cannot be reproduced by a linear combination of the first epoch spectrum and a host galaxy model matching the GROND host photometry.

Whatever causes the blue drop, it has a high optical depth; the most likely cause of variation of the blue feature from 8 h to 33 h is then variation of that optical depth perpendicular to the line of sight, combined with a significant growth of the emitting area we see, as explored for GRB 021004 by Starling et al. (2005). To illustrate this, we use the standard expressions for the expansion of the GRB blast wave in the pre-jet break phase (e.g. Wijers & Galama 1999; Zhang & Mészáros 2004). Since material close to the GRB will be severely affected by its radiation, we assume the absorber is many parsecs from the explosion and does not interact with the blast wave. This is consistent with distances inferred from variable fine-structure lines for other bursts (e.g. Vreeswijk et al. 2007; D'Elia et al. 2007; Vreeswijk et al. 2011; De Cia et al. 2012). The X-ray and UV afterglow may destroy dust out to ~100 pc, but this is not always the case as discussed in Fruchter et al. (2001). Because of the blast wave slowing down, relativistic beaming decreases strongly and we see the emitting area expand: its size scales as $(\gamma ct)^2$, and since in this phase $\gamma \propto t^{-3/8}$, as $t^{5/4}$. Between 8 h and 33 h it therefore expands by about a factor of 6. The fraction of flux that penetrates the absorber near the centre of the feature is at most 5–10% at both epochs. This means that the absorber is big enough still to cover at least 90% of the emitting region at the second epoch, or it is even bigger and the transmitted fraction merely indicates that the optical depth is a few, so a small percentage of the light filters through. The blueward shift of the turnover could either indicate a decrease in average optical depth of the absorber while the area illuminated by the photosphere grows or, less likely, some light reaching us unabsorbed via a small fraction of holes in the absorber.

The alternative explanation of an extreme 2175-Å bump appears less likely as a similar strong bump is not observed anywhere in the MW (Fitzpatrick & Massa 2007).

We note that Fynbo et al. (2009) report an unexplained flux drop in the blue of the afterglow of GRB 070318. This event is discussed in more detail in Watson (2009). This flux drop can also be well reproduced by the Goobar (2008) multiple scattering scenario.

We note that steep UV extinction, albeit less extreme than what we see here, is also seen towards the MW bulge, the central region of M 31 and towards several AGN (e.g. Fynbo et al. 2013; Nataf et al. 2013; Jiang et al. 2013; Dong et al. 2014; Leighly et al. 2014).

4.2. Absorption lines

The metal lines detected in the spectrum are strong, but not unusually strong for a GRB afterglow. The line-strength parameter defined in de Ugarte Postigo et al. (2012) is −0.11 ± 0.15, which implies average line-strengths compared to the sample of Fynbo et al. (2009).

In contrast to this, the absorption lines from excited hydrogen and helium are very unusual. To our knowledge, they have never been detected before in a GRB afterglow spectrum and they are not detected in the composite afterglow spectrum presented in Christensen et al. (2011) down to a limit of about 80 mÅ for Hβ and He I$^*\lambda$3889 (3σ). We have explored whether the population of the excited states of H and He can be explained by the GRB afterglow UV photons exciting a neutral absorption cloud at a distance of 50−500 pc away from the burst. Such an UV pumping model can naturally explain the observations of excited states of ions such as Fe II and Ni II observed along several GRB sightlines (Prochaska et al. 2006; Vreeswijk et al. 2007; D'Elia et al. 2007). We closely follow the methodology of Vreeswijk et al. (2013), which includes both excitation and ionization of the relevant ions (H and He in this case) and a solar helium abundance is assumed. Varying the distance and the initial neutral hydrogen column density over a reasonable range, we find that the population of the excited state of H does not reach above 10^{11} atoms cm^{-2}, while the observed value is almost 10^{14} cm^{-2}. For He I* the difference is less dramatic, but the modelled population is still at least a factor of 10 below the observed value. Therefore, we conclude that excitation by GRB afterglow photons of a nearby neutral absorber is not a viable explanation for the presence of the Balmer and HeI* absorption lines.

It might be that a dense absorber is situated close to the GRB, and is being ionized by it (see also Lazzati & Perna 2002; Prochaska et al. 2008; Krongold & Prochaska 2013). In many astrophysical environments, including quasars and AGN, He1* is populated by recombination, rather than pumping (see e.g. Leighly et al. 2011, for a quasar application). In that case, we would expect to see He I* only if sufficient He$^+$ could recombine to the $n = 2$ level after the GRB. The timescale for recombination to the triplet state for helium is $\sim 1.5 \times 10^5/n_e$ years, and hence even for very high densities n it is difficult to understand how the observed column densities can be achieved before the time of the first X-shooter spectrum.

A third explanation is that the sightline happens to intersect a region in the host galaxy with the observed column densities, caused by an ionizing source different from the GRB, e.g. a massive star or cluster of stars (see also Watson et al. 2013; Krongold & Prochaska 2013). Absorption lines from excited He I* are detected in the ISM of young clusters in the Milky Way. The lines are here formed in H II region around the hot stars. The EW of the He I*λ3889 line measured in the interstellar clouds in front of the Trapezium in Orion is 0.12 Å (Oudmaijer et al. 1997). The strength of the He I*λ3889 line towards GRB 140506A is hence 5 times stronger than that seen towards the Trapezium in Orion. The EW of the He I*λ10833 line is not given in Oudmaijer et al. (1997), but judging from their Fig. 6 it is 3−5 times higher than for the He I*λ3889 line, i.e. a similar ratio to what we see. Evans et al. (2005) report that He I*λ3889 is seen towards many stars in their study of three clusters (NGC 6611, NGC 3293 and NGC 4755) that still contain O and/or B stars, but with large spatial variations. In addition, the strong absorption often detected in the X-ray afterglows of GRBs has been argued to originate from ionized helium in the natal H II of the GRB progenitor star (Watson et al. 2013).

To explore this scenario we have performed photoionization modelling using Cloudy (Ferland et al. 2013) roughly appropriate for a large H II region and accompanying photo-dissociation region (PDR) illuminated by a star cluster. We used a spectral energy distribution consisting of a 5 Myr starburst (Bruzual & Charlot 2003) with added soft X-ray emission to approximate the the emission of the O stars (Sciortino et al. 1990). We assumed constant pressure, and used solar abundances with no dust. We found that we were able to easily reproduce the observed He I* column density in the H II region of illuminated gas slab, as expected, provided that the ionization parameter was high enough (e.g. Leighly et al. 2011). The Balmer absorption occurred in the partially ionized zone/photodisscociation region beyond the Strömgren sphere. The Balmer absorption can only be matched if there is a very high density at the illuminated face, around $\log n/\mathrm{cm}^{-3} = 7.75$ corresponding to $\log n/\mathrm{cm}^{-3} \sim 8.25$ in the Balmer-line absorbing gas; when the density is high, Lyman-α scattering populates the first excited state in hydrogen. These values are much higher than typical for Galactic H II regions ($n \sim 10^3\,\mathrm{cm}^{-3}$), but such densities are found, e.g. in ultra compact H II regions (Churchwell 2002) and photodisscociation regions (Hollenbach & Tielens 1997). The separation between the location of the absorption for the different ions explains the different line widths.

The possible absorption line from CH^+ is strong, but given the correlation with the hydrogen column density seen in the MW (Smoker et al. 2014, their Fig. 3) it is not unreasonably strong given the very large hydrogen column densities typically probed by GRB sightlines (Jakobsson et al. 2006; Fynbo et al. 2009).

4.3. Implications for dark GRBs

It is intriguing that if this afterglow had been located at a more typical redshift of $z \sim 2$ the flux drop would have been located in the observed J band and the burst would have been extremely dark in the observed optical band despite being located behind a relatively modest amount of dust with $A_V \sim 1$. Hence, the effect that causes the unusual spectral shape in the afterglow of GRB 140506A may be important for the understanding of the dark burst phenomenon (Fynbo et al. 2001; Jakobsson et al. 2004a; Greiner et al. 2011; Krühler et al. 2011; Rossi et al. 2012; Perley et al. 2013).

5. Conclusions

In summary we have analysed the afterglow spectrum of GRB 140506A. The spectrum has two peculiar properties: i) an unusual extinction signature with the very strong and variable flux-drop below 8000 Å (4000 Å in the restframe); and ii) absorption lines from exited hydrogen and helium. We think the most likely scenario consistent with the observations is a sightline passing through several distinct regions. The absorption from He I* originates from an H II region, the balmer absorption in the associated partially ionized zone/photodissociation zone, and the extinction is caused by a very dense distribution of dust most likely associated with the gas causing the metal and molecular line absorption (e.g. Ca I, Ca II, CH^+). The closest local analogue to the region causing the dust extinction is probably the sightline to SN 2014J in in the starburst galaxy M 82: along this sightline similar extinction is seen (Amanullah et al. 2014). Furthermore, similar absorption line properties are also seen, e.g. strong calcium absorption and absorption from CH^+ (Ritchey et al. 2014). Sightlines like these may be responsible for turning some bursts into dark bursts.

It is somewhat uncomfortable that the two peculiarities of the sightline towards GRB 140506A do not seem to have a common explanation, but to the best of our judgement this is how the situation seems to be. Whatever the correct interpretation of the steep UV extinction is, it is promising that the phenomenon apparently is seen in several other types of objects, i.e. AGN (Fynbo et al. 2013; Jiang et al. 2013; Leighly et al. 2014), SNe (Goobar 2008; Amanullah et al. 2014) and towards the centre of M 31 (Dong et al. 2014). The outlook for a definitive solution to the mystery is hence good.

Acknowledgements. We are grateful for a very constructive report from an anonymous referee. We are also grateful for helpful discussions with Ariel Goobar, Rene Oudmaijer, Moire Prescott, Kristian Finlator, Sebastian Hönig and J. Xavier Procaska. We are also grateful to the wider X-shooter GRB follow-up team and the staff at the La Silla Paranal Observatory without which this kind of research would not be possible. The Dark Cosmology Centre is funded by the DNRF. The research leading to these results has received funding from the European Research Council under the European Union's Seventh Framework Programme (FP7/2007–2013)/ERC Grant agreement no. EGGS-278202. S. Schulze acknowledges support from CONICYT-Chile FONDECYT 3140534, Basal-CATA PFB-06/2007, and Project IC120009 "Millennium Institute of Astrophysics (MAS)" of Iniciativa Científica Milenio del Ministerio de Economía, Fomento y Turismo. The research activity of Ad.U.P. and C.T. is supported by Spanish research project AYA2012-39362-C02-02. Ad.U.P. acknowledges support by the European Commission under the Marie Curie Career Integration Grant programme (FP7-PEOPLE-2012-CIG 32230). Part of the funding for GROND (both hardware as well as personnel) was generously granted from the Leibniz-Prize to Prof. G. Hasinger (DFG grant HA 1850/28-1). P.S. acknowledges support through the Sofja Kovalevskaja Award from the Alexander von Humboldt Foundation of Germany. D.M. acknowledges support from the Instrument center for Danish Astrophysics (IDA)

References

Aihara, H., Allende Prieto, C., An, D., et al. 2011, ApJS, 193, 29
Amanullah, R., Goobar, A., Johansson, J., et al. 2014, ApJ, 788, L21
Bruzual, G., & Charlot, S. 2003, MNRAS, 344, 1000
Christensen, L., Fynbo, J. P. U., Prochaska, J. X., et al. 2011, ApJ, 727, 73
Churchwell, E. 2002, ARA&A, 40, 27
Covino, S., Melandri, A., Salvaterra, R., et al. 2013, MNRAS, 432, 1231
De Cia, A., Ledoux, C., Fox, A. J., et al. 2012, A&A, 545, A64
De Cia, A., Ledoux, C., Savaglio, S., Schady, P., & Vreeswijk, P. M. 2013, A&A, 560, A88
de Ugarte Postigo, A., Fynbo, J. P. U., Thöne, C. C., et al. 2012, A&A, 548, A11
D'Elia, V., Fiore, F., Meurs, E. J. A., et al. 2007, A&A, 467, 629
D'Elia, V., Fynbo, J. P. U., Goldoni, P., et al. 2014, A&A, 564, A38
Dong, H., Li, Z., Wang, Q. D., et al. 2014, ApJ, 785, 136
Dressler, A., Bigelow, B., Hare, T., et al. 2011, PASP, 123, 288
Elíasdóttir, Á., Fynbo, J. P. U., Hjorth, J., et al. 2009, ApJ, 697, 1725
Ellison, S. L., Vreeswijk, P., Ledoux, C., et al. 2006, MNRAS, 372, L38
Evans, C. J., Smartt, S. J., Lee, J.-K., et al. 2005, A&A, 437, 467
Ferland, G. J., Porter, R. L., van Hoof, P. A. M., et al. 2013, Rev. Mex. Astron. Astrofis., 49, 137
Fitzpatrick, E. L., & Massa, D. 2007, ApJ, 663, 320
Friis, M., De Cia, A., Fynbo, J. P. U., et al. 2014, MNRAS, submitted
Fruchter, A., Krolik, J. H., & Rhoads, J. E. 2001, ApJ, 563, 597
Fynbo, J. U., Jensen, B. L., Gorosabel, J., et al. 2001, A&A, 369, 373
Fynbo, J. P. U., Starling, R. L. C., Ledoux, C., et al. 2006, A&A, 451, L47
Fynbo, J., Vreeswijk, P., Jakobsson, P., et al. 2007, The Messenger, 130, 43
Fynbo, J. P. U., Jakobsson, P., Prochaska, J. X., et al. 2009, ApJS, 185, 526
Fynbo, J. P. U., Krogager, J.-K., Venemans, B., et al. 2013, ApJS, 204, 6
Fynbo, J. P. U., Tanvir, N. R., Jakobsson, P., et al. 2014, GRB Coordinates Network, 16217, 1
Goldoni, P., Royer, F., François, P., et al. 2006, in SPIE Conf., 6269
Golenetskii, S., Aptekar, R., Frederiks, D., et al. 2014, GRB Coordinates Network, 16223, 1
Gompertz, B. P., Burrows, D. N., Cenko, S. B., et al. 2014, GRB Coordinates Network, 16214, 1
Goobar, A. 2008, ApJ, 686, L103
Greiner, J., Bornemann, W., Clemens, C., et al. 2008, PASP, 120, 405
Greiner, J., Krühler, T., Klose, S., et al. 2011, A&A, 526, A30
Hollenbach, D. J., & Tielens, A. G. G. M. 1997, ARA&A, 35, 179
Jakobsson, P., Hjorth, J., Fynbo, J. P. U., et al. 2004a, ApJ, 617, L21
Jakobsson, P., Hjorth, J., Fynbo, J. P. U., et al. 2004b, A&A, 427, 785
Jakobsson, P., Fynbo, J. P. U., Ledoux, C., et al. 2006, A&A, 460, L13
Jenke, P. 2014, GRB Coordinates Network, 16220, 1
Jiang, P., Zhou, H., Ji, T., et al. 2013, AJ, 145, 157
Kennicutt, Jr., R. C. 1998, ARA&A, 36, 189
Krongold, Y., & Prochaska, J. X. 2013, ApJ, 774, 115
Krühler, T., Küpcü Yoldaş, A., Greiner, J., et al. 2008, ApJ, 685, 376
Krühler, T., Greiner, J., Schady, P., et al. 2011, A&A, 534, A108
Krühler, T., Ledoux, C., Fynbo, J. P. U., et al. 2013, A&A, 557, A18
Lazzati, D., & Perna, R. 2002, MNRAS, 330, 383
Leighly, K. M., Dietrich, M., & Barber, S. 2011, ApJ, 728, 94
Leighly, K. M., Terndrup, D. M., Baron, E., et al. 2014, ApJ, 788, 123
Li, A., Liang, S. L., Kann, D. A., et al. 2008, ApJ, 685, 1046

Markwardt, C. B., Barthelmy, S. D., Baumgartner, W. H., et al. 2014, GRB Coordinates Network, 16218, 1
Modigliani, A., Goldoni, P., Royer, F., et al. 2010, in SPIE Conf. Ser. 7737
Nataf, D. M., Gould, A., Fouqué, P., et al. 2013, ApJ, 769, 88
Oudmaijer, R. D., Drew, J. E., Barlow, M. J., Crawford, I. A., & Proga, D. 1997, MNRAS, 291, 110
Pei, Y. C. 1992, ApJ, 395, 130
Perley, D. A., Bloom, J. S., Klein, C. R., et al. 2010, MNRAS, 406, 2473
Perley, D. A., Levan, A. J., Tanvir, N. R., et al. 2013, ApJ, 778, 128
Prochaska, J. X., Chen, H.-W., & Bloom, J. S. 2006, ApJ, 648, 95
Prochaska, J. X., Chen, H.-W., Dessauges-Zavadsky, M., & Bloom, J. S. 2007, ApJ, 666, 267
Prochaska, J. X., Dessauges-Zavadsky, M., Ramirez-Ruiz, E., & Chen, H.-W. 2008, ApJ, 685, 344
Prochaska, J. X., Sheffer, Y., Perley, D. A., et al. 2009, ApJ, 691, L27
Ritchey, A. M., Welty, D. E., Dahlstrom, J. A., & York, D. G. 2014, ApJ, submitted [arXiv:1407.5723]
Rossi, A., Klose, S., Ferrero, P., et al. 2012, A&A, 545, A77
Savaglio, S. 2006, New J. Phys., 8, 195
Schady, P., Dwelly, T., Page, M. J., et al. 2012, A&A, 537, A15
Sciortino, S., Vaiana, G. S., Harnden, Jr., F. R., et al. 1990, ApJ, 361, 621
Siegel, M. H., & Gompertz, B. P. 2014, GRB Coordinates Network, 16219, 1
Skrutskie, M. F., Cutri, R. M., Stiening, R., et al. 2006, AJ, 131, 1163
Smoker, J., Ledoux, C., Jehin, E., et al. 2014, MNRAS, 438, 1127
Sparre, M., Hartoog, O. E., Krühler, T., et al. 2014, ApJ, 785, 150
Starling, R. L. C., Wijers, R. A. M. J., Hughes, M. A., et al. 2005, MNRAS, 360, 305
Thöne, C. C., Fynbo, J. P. U., Goldoni, P., et al. 2013, MNRAS, 428, 3590
Tody, D. 1993, in Astronomical Data Analysis Software and Systems II, eds. R. J. Hanisch, R. J. V. Brissenden, & J. Barnes, ASP Conf. Ser., 52, 173
Vernet, J., Dekker, H., D'Odorico, S., et al. 2011, A&A, 536, A105
Vreeswijk, P. M., Ledoux, C., Smette, A., et al. 2007, A&A, 468, 83
Vreeswijk, P. M., Ledoux, C., Smette, A., et al. 2011, A&A, 532, C3
Vreeswijk, P. M., Ledoux, C., Raassen, A. J. J., et al. 2013, A&A, 549, A22
Wang, L. 2005, ApJ, 635, L33
Watson, D. 2009, in Cosmic Dust – Near and Far, eds. T. Henning, E. Grün, & J. Steinacker, ASP Conf. Ser., 414, 277
Watson, D., Fynbo, J. P. U., Ledoux, C., et al. 2006, ApJ, 652, 1011
Watson, D., Zafar, T., Andersen, A. C., et al. 2013, ApJ, 768, 23
Wijers, R. A. M. J., & Galama, T. J. 1999, ApJ, 523, 177
Xiang, F. Y., Li, A., & Zhong, J. X. 2011, ApJ, 733, 91
Zafar, T., Watson, D., Fynbo, J. P. U., et al. 2011, A&A, 532, A143
Zhang, B., & Mészáros, P. 2004, Int. J. Mod. Phys. A, 19, 2385

[1] Dark Cosmology Centre, Niels Bohr Institute, Copenhagen University, Juliane Maries Vej 30, 2100 Copenhagen Ø, Denmark
e-mail: jfynbo@dark-cosmology.dk
[2] European Southern Observatory, Alonso de Córdova 3107, Vitacura, Casilla 19001, Santiago 19, Chile
[3] Homer L. Dodge Department of Physics and Astronomy, The University of Oklahoma, 440 West Brooks Street, Norman, OK 73019, USA
[4] Department of Particle Physics and Astrophysics, Weizmann Institute of Science, 76100 Rehovot, Israel
[5] Instituto de Astrofísica, Facultad de Física, Pontificia Universidad Caólica de Chile, Av. Vicuña Mackenna 4860, Santiago, Chile
[6] Millennium Institute of Astrophysics, Vicuña Mackenna 4860, 7820436 Macul, Santiago, Chile
[7] Institut d'Astrophysique de Paris, CNRS-UPMC, UMR 7095, 98bis Bd Arago, 75014 Paris, France
[8] Astronomical Institute Anton Pannekoek, University of Amsterdam, PO Box 94249, 1090 GE Amsterdam, the Netherlands
[9] Max-Planck-Institut für extraterrestrische Physik, Giessenbachstrasse, 85748 Garching, Germany
[10] Centre for Astrophysics and Cosmology, Science Institute, University of Iceland, Dunhagi 5, 107 Reykjavík, Iceland
[11] INAF–Brera Astronomical Observatory, via Bianchi 46, 23807 Merate (LC), Italy
[12] INAF–Osservatorio Astronomico di Roma, via Frascati 33, 00040 Monteporzio Catone, Italy
[13] ASI-Science Data Center, via del Politecnico snc, 00133 Rome, Italy
[14] Laboratoire Galaxies Étoiles Physique et Instrumentation, Observatoire de Paris, 5 place Jules Janssen, 92195 Meudon, France
[15] APC, Astroparticule et Cosmologie, Univ. Paris Diderot, CNRS/IN2P3, CEA/Irfu, Obs. de Paris, Sorbonne Paris Cité, 10 rue Alice Domon et Léonie Duquet, 75205 Paris Cedex 13, France
[16] Laboratoire GEPI, Observatoire de Paris, CNRS-UMR 8111, Univ. Paris Diderot, 5 place Jules Janssen, 92195 Meudon, France
[17] Faculty of Mathematics and Physics, University of Ljubljana, Jadranska ulica 19, 1000 Ljubljana, Slovenia
[18] Thüringer Landessternwarte Tautenburg, Sternwarte 5, 07778 Tautenburg, Germany
[19] Department of Physics, University of Warwick, Coventry CV4 7AL, UK
[20] European Southern Observatory, Karl-Schwarzschildstrasse 2, 85748 Garching, Germany
[21] Instituto de Astrofísica de Andalucía, Glorieta de la Astronomía s/n, 18008 Granada, Spain
[22] Scuola Normale Superiore di Pisa, Piazza dei Cavalieri 7, 56126 Pisa, Italy
[23] Department of Physics and Astronomy, University of Leicester, University Road, Leicester LE1 7RH, UK